



UNIVERSITY OF LEEDS

This is a repository copy of *Morphology of bile salts micelles and mixed micelles with lipolysis products, from scattering techniques and atomistic simulations.*

White Rose Research Online URL for this paper:
<https://eprints.whiterose.ac.uk/180879/>

Version: Accepted Version

Article:

Pabois, O orcid.org/0000-0001-5307-7149, Ziolek, RM, Lorenz, CD et al. (11 more authors) (2021) Morphology of bile salts micelles and mixed micelles with lipolysis products, from scattering techniques and atomistic simulations. *Journal of Colloid and Interface Science*, 587. pp. 522-537. ISSN 0021-9797

<https://doi.org/10.1016/j.jcis.2020.10.101>

© 2020 Elsevier Inc. This is an author produced version of a paper published in *Journal of Colloid and Interface Science*. Uploaded in accordance with the publisher's self-archiving policy. This manuscript version is made available under the Creative Commons CC-BY-NC-ND 4.0 license <http://creativecommons.org/licenses/by-nc-nd/4.0/>

Reuse

This article is distributed under the terms of the Creative Commons Attribution-NonCommercial-NoDerivs (CC BY-NC-ND) licence. This licence only allows you to download this work and share it with others as long as you credit the authors, but you can't change the article in any way or use it commercially. More information and the full terms of the licence here: <https://creativecommons.org/licenses/>

Takedown

If you consider content in White Rose Research Online to be in breach of UK law, please notify us by emailing eprints@whiterose.ac.uk including the URL of the record and the reason for the withdrawal request.



eprints@whiterose.ac.uk
<https://eprints.whiterose.ac.uk/>

Morphology of bile salts micelles and mixed micelles with lipolysis products, from scattering techniques and atomistic simulations

Olivia Pabois^{a, b}, Robert M. Ziolk^c, Christian D. Lorenz^c, Sylvain Prévost^a, Najet Mahmoudi^d, Maximilian W. A. Skoda^d, Rebecca J. L. Welbourn^d, Margarita Valero^e, Richard D. Harvey^f, Myriam M.-L. Grundy^g, Peter J. Wilde^h, Isabelle Grillo^a, Yuri Gerelli^{a, i*}, Cécile A. Dreiss^{b*}

^a Institut Laue-Langevin, Grenoble 38000, France

^b Institute of Pharmaceutical Science, King's College London, London SE1 9NH, United Kingdom

^c Department of Physics, King's College London, London WC2R 2LS, United Kingdom

^d ISIS Neutron & Muon Source, STFC Rutherford Appleton Laboratory, Didcot OX11 0QX, United Kingdom

^e Department of Physical Chemistry, University of Salamanca, Salamanca 37007, Spain

^f Department of Pharmaceutical Chemistry, University of Vienna, Vienna A-1090, Austria

^g PEGASE, INRAE, Institut Agro, Saint Gilles 35590, France

^h Quadram Institute Bioscience, Norwich Research Park, Norwich NR4 7UA, United Kingdom

ⁱ Department of Life and Environmental Sciences, Polytechnic University of Marche, Ancona 60131, Italy

E-mail addresses:

olivia.pabois@kcl.ac.uk; rob.ziolk@kcl.ac.uk; chris.lorenz@kcl.ac.uk; prevost@ill.fr;
najet.mahmoudi@stfc.ac.uk; maximilian.skoda@stfc.ac.uk; becky.welbourn@stfc.ac.uk;
mvalero@usal.es; richard.harvey@univie.ac.at; myriam.grundy@inrae.fr;
peter.wilde@quadram.ac.uk; y.gerelli@univpm.it; cecile.dreiss@kcl.ac.uk

Corresponding authors:

Cécile A. Dreiss:

King's College London
Institute of Pharmaceutical Science
Franklin-Wilkins Building
150 Stamford Street
SE1 9NH London, UK
Tel: +44 207 848 3766

Yuri Gerelli:

Polytechnic University of Marche
Department of Life and Environmental Sciences
6, via Brecce Bianche
60131 Ancona, Italy
Tel: +39 071 220 4608

Supporting information

Molecular structures

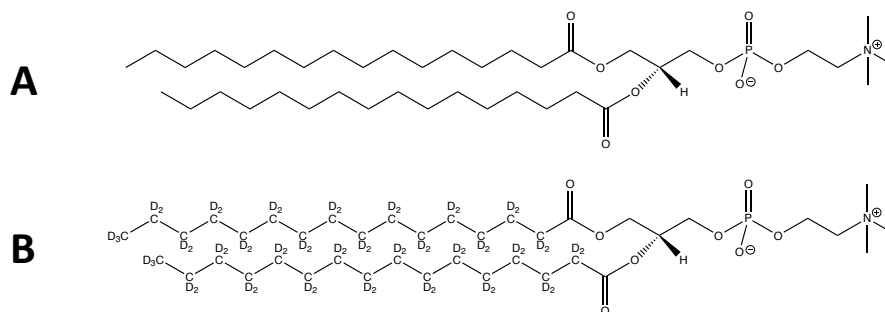
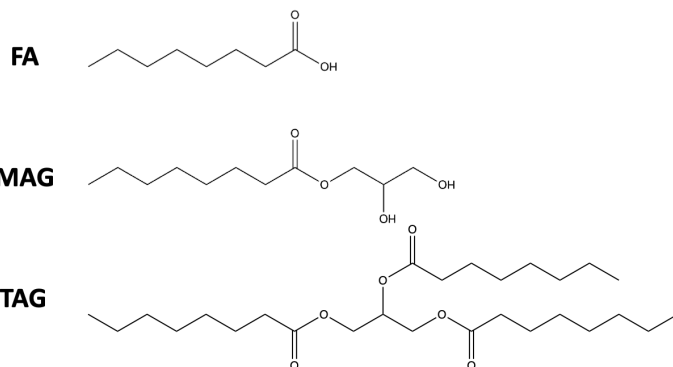


Figure S1: Structures of DPPC (A) and d_{62} -DPPC (B).

C8:0



C18:1

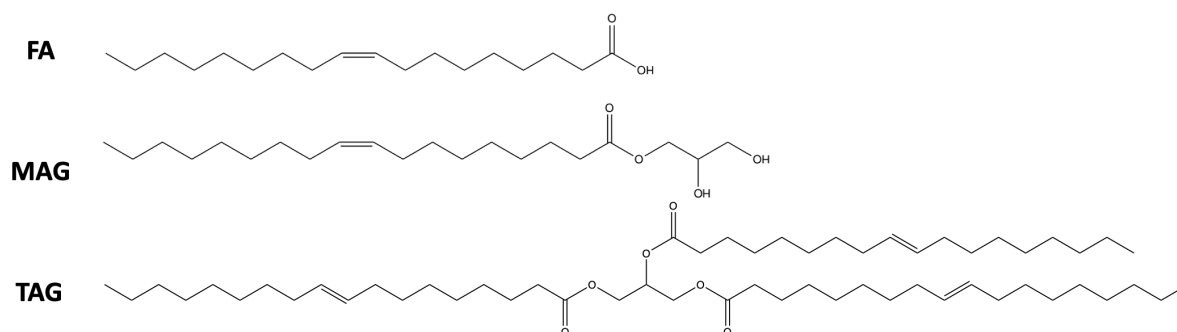


Figure S2: Structures of caprylic acid (C8:0 FA), monocaprylin (C8:0 MAG), tricaprylin (C8:0 TAG), oleic acid (C18:1 FA), monoolein (C18:1 MAG) and triolein (C18:1 TAG).

Micro-differential scanning calorimetry measurements: liposomes phase transition temperature

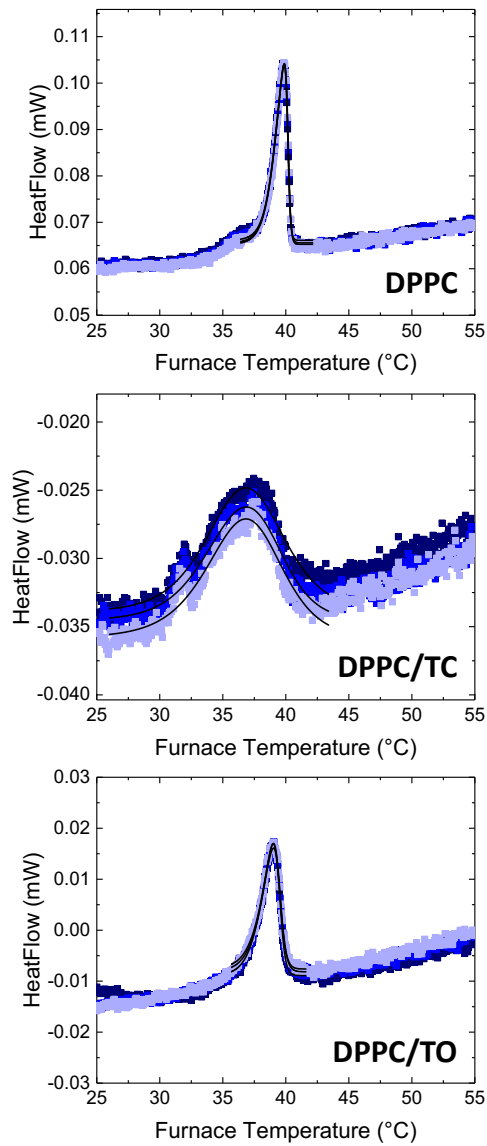


Figure S3: Micro-differential scanning calorimetry thermograms (cooling curves, 0.5 K/min cooling rate) showing the gel-to-fluid transition of liposomes: DPPC, DPPC/TC, DPPC/TO. The liposomes phase transition temperature is taken here as the temperature value at which the peak maximum is reached. Each measurement was reproduced three times, and each of them is shown for each liposome.

Quartz-crystal microbalance measurements: protocol of SLB formation

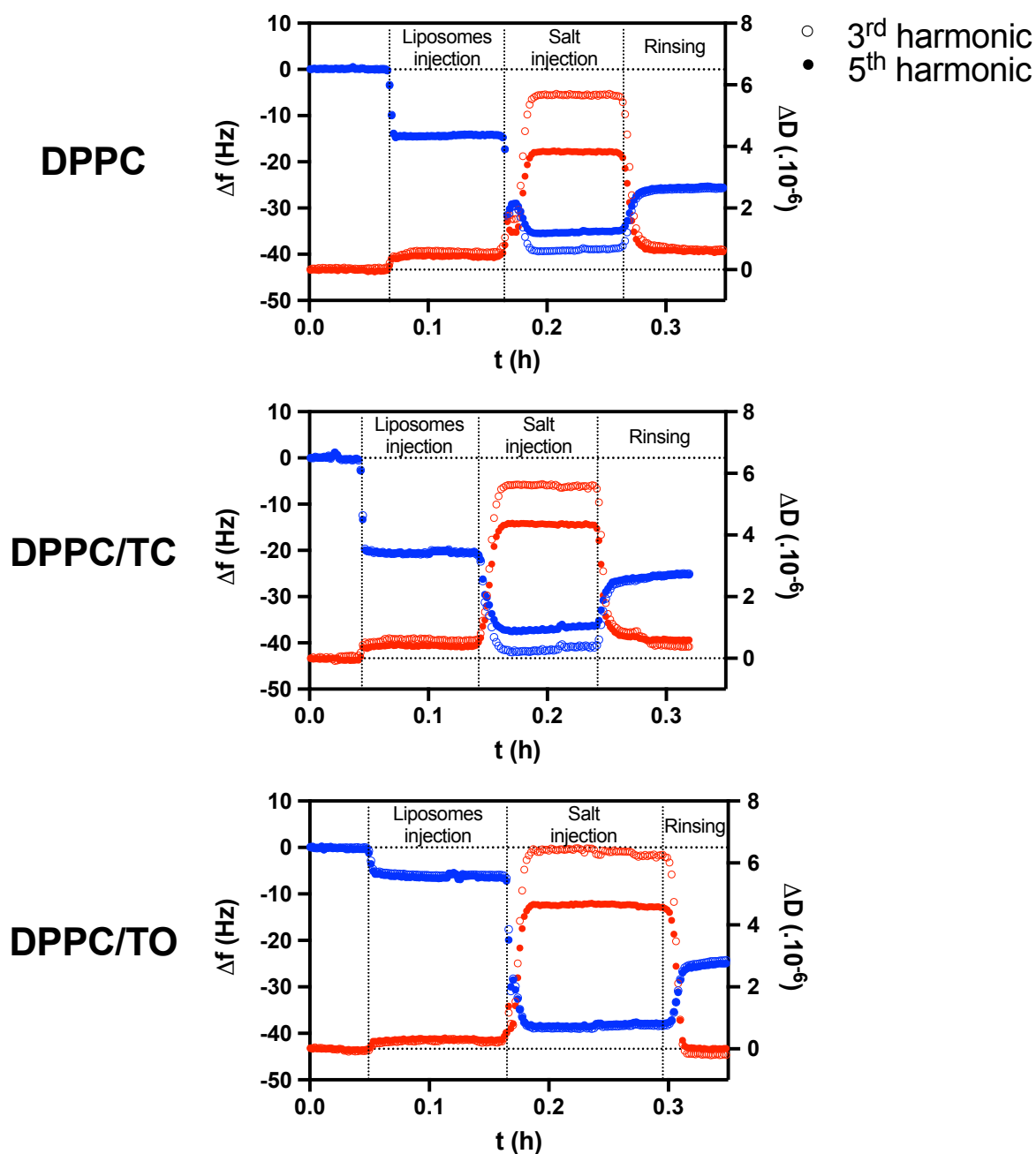


Figure S4: Time-dependent evolution of the (\bullet) resonance frequency (Δf) and (\circ) energy dissipation factor (ΔD) measured by quartz-crystal microbalance with dissipation monitoring [1], upon formation of a SLB: DPPC, DPPC/TC, DPPC/TO, in ultrapure water, through liposomes fusion (at $50 \pm 2^\circ\text{C}$). Liposomes, followed by salt (0.5 M NaCl), were injected into the chamber, which was finally rinsed with ultrapure water to remove the lipid vesicles remaining intact at the interface and in the bulk. For readability purposes, resonance frequencies and energy dissipation factors obtained for the 3rd and 5th harmonics only are shown here. A frequency shift of around -25 Hz typically denotes the effective formation of a stable lipid membrane [2]. Each experiment was reproduced twice, and a representative measurement was selected for each SLB.

Quartz-crystal microbalance with dissipation monitoring measurements [1] were performed prior to NR experiments in order to define the protocol of formation of the SLB described in the “neutron reflectometry” section. Changes in resonance frequency (Δf), which correlates with the adsorbed mass [3], and in energy dissipation factor (ΔD) were recorded simultaneously over time. For each composition, the injection of liposomes leads to a first decrease in resonance frequency (Δf) (and, to a lower extent, to an increase in energy dissipation factor (ΔD)), indicating lipid vesicles adsorption onto the silica-coated support (Figure S4). The addition of salt results in a second, much higher decrease in resonance frequency (and in an increase in energy dissipation factor), which implies the formation of the SLB. Upon rinsing, surface-adsorbed liposomes are removed, thus leading to a rise to around -25 Hz and to a drop to less than 1×10^{-6} for, respectively, the resonance frequency and energy dissipation factor – which are values characteristic of the formation of a homogeneous and rigid SLB [2].

Scattering measurements: instrument configurations

Neutron reflectometry (NR). The INTER time-of-flight reflectometer employed in this study (ISIS pulsed neutron source, STFC Rutherford Appleton Laboratory, Didcot, UK) [4] uses an incoming polychromatic neutron beam with wavelengths (λ) ranging from 1.8 to 17 Å, with a 3% $\Delta q_z/q_z$ resolution, where q_z is the scattering vector perpendicular to the surface (with $q_z = \frac{4\pi}{\lambda} \sin \vartheta_i$). Two different incident angles (ϑ_i , with $\theta_1 = 0.7^\circ$ and $\theta_2 = 2.3^\circ$) were employed to obtain q_z values ranging from 0.01 to 0.3 Å⁻¹ and, for the two angles, the illuminated area (footprint) was kept constant, within the area of the liquid cell. Reflectivity (R), which is the ratio between the reflected and incident intensities, was measured as a function of q_z in this range. NR data were converted to reflectivity curves $R(q_z)$ using the manipulation and analysis toolkit for instrument data (MANTID) [5].

Small-angle X-ray scattering (SAXS). The ID02 instrument employed in this study (ESRF, Grenoble, France) [6] was equipped with a charge-coupled device-based Rayonix MX-170HS detector, and configured with an incoming monochromatic X-ray beam of wavelength $\lambda = 1$ Å (12.46 keV X-ray energy) and resolution $\Delta\lambda/\lambda = 0.015\%$. Two fixed sample-to-detector distances (1 and 2 m) were used, thus allowing values of the scattering vector (q , with $q = \frac{4\pi}{\lambda} \sin \vartheta$, with 2ϑ the scattering angle) ranging from 0.015 to 0.8 Å⁻¹ to be obtained.

Data were corrected for dark current, flat field, incoming flux and transmitted beam measured simultaneously with the scattering. Ten measurements were averaged after verifying that no change due to radiation damage occurred. Contribution of the solvent-filled capillary was subtracted. The absolute scale was determined using the plateau intensity level of water (at $1.63 \times 10^{-2} \text{ cm}^{-1}$, at 298 K).

Small-angle neutron scattering (SANS). The SANS2D data obtained in this study for BS micelles and mixed micelles (ISIS pulsed neutron source, STFC Rutherford Appleton Laboratory, Didcot, UK) [7] were acquired with a polychromatic incident beam of wavelength (λ) ranging between 1.75 and 16.5 Å and with a fixed instrument setup of $L1 = L2 = 4$ m (where $L1$ is the collimation length and $L2$ the sample-to-detector distance); a simultaneous q -range of 0.004 to 1 Å⁻¹ was achieved using two 1 m² detectors at 2.4 and 4 m from the sample, with a q -resolution varying from ca. 2% at the highest q -values to ca. 19% with decreasing q -values, calculated using the Mildner Carpenter equation [8]. The D33 data obtained in this study for

BS micelles and TAG-incorporating liposomes (ILL, Grenoble, France) [9] were recorded with a monochromatic neutron beam with an incident wavelength of $\lambda = 6 \text{ \AA}$ (with a 10% $\Delta\lambda/\lambda$ resolution) and three fixed sample-to-detector distances ($D = 2, 5$ and 12 m), as well as with $\lambda = 13 \text{ \AA}$ and $D = 12 \text{ m}$, thus obtaining q values ranging from 1.5×10^{-3} to 0.47 \AA^{-1} .

Detector images were radially averaged and corrected from the scattering of the empty cell and D_2O background. Detector efficiency corrections and data normalisation to an appropriate standard were done using MANTID (for SANS2D data) [5] and the large array manipulation program (LAMP) (for D33 data) [10].

Scattering measurements: data analysis

Calculation of the electron and neutron *SLD*. The electron and neutron *SLD* of a molecule are defined as follows:

$$\text{electron SLD} = r_e \frac{\sum x_i Z_i}{v_m} \quad (\text{S1})$$

$$\text{neutron SLD} = \frac{\sum x_i b_c^i}{v_m} \quad (\text{S2})$$

where x_i is the number of atom i in the molecule, v_m the molecular volume of the molecule, r_e the classical radius of the electron, Z_i the atomic number of the atom i , and b_c^i the coherent scattering length of the atom i (values of coherent scattering lengths are tabulated [11,12]).

Neutron reflectometry (NR). Data analysis was performed with the Aurore software [13] and a global fitting procedure was applied for compatible data sets. Briefly, the SLB was divided into four layers, each characterised by a specific thickness (t), *SLD*, amount of water (f_{water}) and interfacial roughness (σ). Because of the instrumental geometry used, the first two (upper) layers in the SLB model correspond to the head groups (in contact with silicon oxide (SiO_x)) and the tails regions of the inner leaflet, while the second two (lower) ones are ascribed to the tails and head groups (in contact with the aqueous phase) of the outer leaflet (see Supporting Information in reference [14]). An additional layer was used to model the native SiO_x layer present on the substrate surface. The result of the NR data analysis is a *SLD* profile along the direction perpendicular to the surface (z), which is directly related to the distribution of each molecular component in this direction.

Small-angle X-ray and neutron scattering (SAXS, SANS)

BS neat and mixed micelles (SAXS, SANS). Data analysis was performed with the SasView software [15]. The intensity $I(q)$ scattered from BS micelles and mixed micelles was fitted to an oblate ellipsoid model combined with a Hayter-Penfold structure factor:

$$I(q) = \Phi_{Micelles} (SLD_{Micelle} - SLD_{Water})^2 P_{Ellipsoid}(q) S_{H-P}(q) \quad (\text{S3})$$

where $\Phi_{Micelles}$ is the micellar volume fraction, $SLD_{Micelle}$ and SLD_{Water} the *SLD* of the BS micelle or mixed micelle and water, respectively, $P_{Ellipsoid}(q)$ the form factor for ellipsoids, and $S_{H-P}(q)$ the Hayter-Penfold structure factor, which describes the interactions between charged

micelles [16,17]. The polydispersity of micellar radii was fixed at 0.2, assuming a lognormal distribution.

TAG-incorporating lipid vesicles (SANS). The intensity $I(q)$ scattered from pure liposomes was fitted to a model that takes into account two vesicle populations of uni- and multi-lamellar vesicles (further detail can be found in [18]). The uni-lamellar lipid vesicles contribution is described by a core/shell structure, with a Schultz distribution for the size, while the multi-lamellar lipid vesicles are described by a core surrounded by multiple lipid bilayer shells, each spaced by an aqueous solvent layer; in the case of multi-lamellar liposomes, the polydispersity is attributed to the variable number of bilayers (or shells) and polydispersity of the solvent layer thickness, also described by a Schultz distribution. The features of the individual bilayers (SLD , thickness and hydration) were described by the same set of parameters for uni- and multi-lamellar vesicles.

For the analysis of BS micelles, knowing that:

$$\Phi_{Micelles} = \Phi_{BS} + \Phi_{Water} = \frac{\Phi_{BS}}{1 - x_{Water}} \quad (S4)$$

and:

$$\begin{aligned} SLD_{Micelle} - SLD_{Water} &= (1 - x_{Water}) SLD_{BS} + x_{Water} SLD_{Water} - SLD_{Water} \\ &= (1 - x_{Water}) (SLD_{BS} - SLD_{Water}) \quad (S5) \end{aligned}$$

where Φ_{BS} and Φ_{Water} are the volume fractions of, respectively, BS and water in micelles, x_{Water} , or $\frac{\Phi_{Water}}{\Phi_{Micelles}}$, the proportion of water in micelles, and SLD_{BS} the SLD of BS, Equation (S3) can be rewritten as follows:

$$I(q) = \Phi_{BS} (1 - x_{Water}) (SLD_{BS} - SLD_{Water})^2 P_{Ellipsoid}(q) S_{H-P}(q) \quad (S6)$$

where $\Phi_{BS} (1 - x_{Water})$ corresponds to the volume fraction parameter returned by the software (referred to as $\Phi_{software}$), when fixing the SLD of BS and water in the software to their calculated value (Table 1). Φ_{BS} is calculated by considering the presence of free unimers in the solution:

$$\Phi_{BS} = \frac{([BS]_{total} - CMC_{BS}) M_{BS}}{\rho_{BS}} \quad (S7)$$

where $[BS]_{total}$ is the total BS concentration in the solution, CMC_{BS} the BS critical micellar concentration, M_{BS} the BS molecular weight, and ρ_{BS} the BS density. The degree of hydration of BS micelles (x_{Water}) is then estimated from the volume fraction fitted. It is worth noting that for the measurement of BS micelles and mixed micelles with SANS, x_{Water} actually corresponds to the extent of hydration of the micellar core, as this technique was found to resolve this part of the aggregate only.

The volume of each BS micelle or mixed micelle ($V_{Micelle}$) was calculated as follows:

$$V_{Micelle} = \frac{4}{3} \pi R_{Pol} R_{Eq}^2 \quad (S8)$$

where R_{Pol} and R_{Eq} are the polar and equatorial radii of the oblate ellipsoid micelle.

The aggregation number (N_{agg}) of the micelles was determined from SAXS by:

$$N_{agg} = \frac{V_{BS}^{Micelle}}{v_{m\ BS}}, \text{ with } V_{BS}^{Micelle} = \frac{4}{3} \pi R_{Pol} R_{Eq}^2 (1 - x_{Water}) \quad (S9)$$

where $V_{BS}^{Micelle}$ is the volume occupied by BS in the hydrated micelle and $v_{m\ BS}$ the molecular volume of each BS ($v_{m\ NaTC} = 0.680 \text{ nm}^3$ [19] and $v_{m\ NaTDC} = 0.658 \text{ nm}^3$ [20]).

The eccentricity of each BS micelle was calculated as follows:

$$\text{Eccentricity} = \sqrt{1 - \frac{R_{Pol}^2}{R_{Eq}^2}} \quad (S10)$$

Therefore, the eccentricity of an ellipsoid varies between 0 and 1, and that of a sphere is 0.

For the analysis of mixed micelles, making the hypothesis that all the additives (FA or MAG) molecules contribute to the formation of mixed aggregates, the volume fractions of the additive (Φ_{FA} and Φ_{MAG}) were calculated considering the absence of free unimers, and the SLD of the objects measured with SANS was fixed to $SLD_{BS/FA \text{ or } BS/MAG}$, with $SLD_{BS/FA \text{ or } BS/MAG} = \frac{1}{\Phi_{BS/FA \text{ or } BS/MAG}} (\Phi_{BS} SLD_{BS} + \Phi_{FA \text{ or } MAG} SLD_{FA \text{ or } MAG})$, where Φ_{BS} and $\Phi_{FA \text{ or } MAG}$ are the volume fractions of, respectively, BS and FA or MAG, SLD_{BS} and $SLD_{FA \text{ or } MAG}$ the SLD of, respectively, BS and FA or MAG, $\Phi_{BS/FA \text{ or } BS/MAG}$ and $SLD_{BS/FA \text{ or } BS/MAG}$ the total volume fraction and total SLD , respectively (Table S2).

The composition of the BS mixed micelles formed upon addition of BS to liposomes being unknown, the *SLD* of the objects probed by SANS was fixed to the *SLD* of BS; this assumption is reasonable since in the ‘ideal’ case where all the lipids, TAG and BS are incorporated into the mixed aggregates (which is not the case here as the systems contain other structures than mixed micelles), the minimum value of *SLD* obtained would be $0.69 \times 10^{-6} \text{ \AA}^{-2}$, which is relatively similar to that of BS ($0.95 \times 10^{-6} \text{ \AA}^{-2}$ for NaTC, and $0.90 \times 10^{-6} \text{ \AA}^{-2}$ for NaTDC).

For the analysis of both BS neat and mixed micelles, all the known parameters (i.e., *SLD* of the objects measured and solvent, salt concentration) were fixed to minimise the variation on the fitted parameters; an error of $\pm 2 \text{ \AA}$ on the fitted radii parameters (R_{Pol} , R_{Eq}) was found. The error on the objects volume ($V_{Micelle\ core}$, $V_{Micelle}$, $V_{Mixed\ micelle\ core}$) and N_{agg} was estimated based on the radii error values.

Type and quantity of FA and MAG used in BS mixed aggregates

Table S1: Type and quantity of additives used in BS mixed micelles

	Additive	[Additive] (% w/w)
FA	Caprylic acid (C8:0)	0.25
		1.50
	Oleic acid (C18:1)	0.10
MAG		0.25
	Monocaprylin (C8:0)	1.30
		0.10
	Monoolein (C18:1)	0.25

Parameters obtained from the analysis of scattering data from BS mixed micelles (with FA or MAG)

Table S2: Concentration of FA (C8:0 or C18:1) or MAG (C8:0 or C18:1) in the sample (*[Additive]*), volume fraction of each component in the micelles (Φ_{BS} , Φ_{FA} , Φ_{MAG}), total volume fraction ($\Phi_{BS/FA \text{ or } BS/MAG} = \Phi_{BS} + \Phi_{FA \text{ or } MAG}$), *SLD* of each component (SLD_{BS} , SLD_{FA} , SLD_{MAG}), total *SLD* ($SLD_{BS/FA \text{ or } BS/MAG} = \frac{1}{\Phi_{BS/FA \text{ or } BS/MAG}} (\Phi_{BS} SLD_{BS} + \Phi_{FA \text{ or } MAG} SLD_{FA \text{ or } MAG})$), for each BS studied: NaTC, NaTDC, with and without 0.15 M NaCl. These parameters were used to fit SANS2D data. While the density of both FA was known (0.91 for C8:0 FA and 0.89 for C18:1 FA), the density of both MAG was assumed to be of similar value and was fixed at 0.90 for the calculation of the volume fractions.

NaTC		[Additive] (% w/w)	Φ_{BS}		Φ_{FA}	Φ_{MAG}	$\Phi_{BS/FA \text{ or } BS/MAG}$		$SLD_{BS/FA \text{ or } BS/MAG}$ ($\cdot 10^{-6}$) (\AA^{-2})	
			No salt	Salt			No salt	Salt	No salt	Salt
			FA	C8 :0			0.25	0.0392	0.0400	0.0031
1.50	0.0386	0.0395			0.0160	-	0.0546	0.0555	0.73	0.73
C18 :1	0.10	0.0393		0.0401	0.0011	-	0.0404	0.0412	0.93	0.93
	0.25	0.0392		0.0400	0.0031	-	0.0423	0.0431	0.89	0.89
MAG	C8 :0	0.25	0.0392	0.0400	-	0.0029	0.0421	0.0429	0.91	0.91
		1.30	0.0387	0.0395	-	0.0142	0.0530	0.0538	0.79	0.79
	C18 :1	0.10	0.0393	0.0401	-	0.0011	0.0404	0.0412	0.93	0.93
		0.25	0.0392	0.0400	-	0.0027	0.0418	0.0427	0.90	0.90

NaTDC		[Additive] (% w/w)	Φ_{BS}		Φ_{FA}	Φ_{MAG}	$\Phi_{BS/FA \text{ or } BS/MAG}$		$SLD_{BS/FA \text{ or } BS/MAG}$ ($\cdot 10^{-6}$) (\AA^{-2})	
			No salt	Salt			No salt	Salt	No salt	Salt
			FA	C8 :0			0.25	0.0387	0.0391	0.0033
1.50	0.0382	0.0386			0.0166	-	0.0548	0.0552	0.68	0.69
C18 :1	0.10	0.0388		0.0392	0.0013	-	0.0401	0.0405	0.87	0.87
	0.25	0.0387		0.0391	0.0029	-	0.0416	0.0420	0.84	0.84
MAG	C8 :0	0.25	0.0387	0.0391	-	0.0027	0.0414	0.0418	0.86	0.86
		1.30	0.0382	0.0386	-	0.0145	0.0527	0.0531	0.75	0.75
	C18 :1	0.10	0.0388	0.0392	-	0.0011	0.0399	0.0403	0.88	0.88
		0.25	0.0387	0.0391	-	0.0027	0.0414	0.0418	0.86	0.86

Parameters obtained from the analysis of scattering data from BS micelles

Table S3: Concentration of BS in the sample ($[BS]$), volume fraction of BS in the micelles (Φ_{BS}), amount of charges in BS micelle, volume fraction fitted by the software ($\Phi_{software}$, also equal to $\Phi_{BS}(1 - x_{Water})$), polar (R_{Pol}) and equatorial (R_{Eq}) radii values of the (oblate) ellipsoid BS micelle, volumes of the BS micelle core ($V_{Micelle\ core}$) and micelle ($V_{Micelle}$), proportion of water in BS micelle core ($x_{Water\ in\ micelles\ core}$) and micelle ($x_{Water\ in\ micelles}$), eccentricity, volume fraction of BS micelles in solution ($\Phi_{Micelles}$), and BS micelle aggregation number (N_{agg}), for each BS studied: NaTC, NaTDC, with and without 0.15 M NaCl. These parameters were obtained from SANS2D (SANS) and ID02 (SAXS) data fitting. In the absence of salt, only SANS data could be fitted and, therefore, only the parameters obtained from the SANS measurements are shown in this table; in the presence of salt, both SANS and SAXS data could be fitted, except the ones obtained at high BS concentrations (i.e., 100 and 200 mM), where strong peaks of interaction are present. To note: below the CMC and where $N_{agg} \sim 1$, the objects probed are unimers rather than micelles but the same terminology (referring to “micelles”) was kept.

Without salt

NaTC

[BS] (mM)	Φ_{BS}	Charges (e)	$\Phi_{Software}$	R_{Pol} (Å)	R_{Eq} (Å)	$V_{Micelle\ core}$ (nm ³)	$x_{Water\ in\ the\ core}$	Eccentricity
25	0.0086	-	0.0080	4 ± 2	10 ± 2	2 ± 1	0.1	0.92 ± 0.09
50	0.0189	4	0.0181	3 ± 2	14 ± 2	3 ± 2	0.04	0.98 ± 0.03
100	0.0394	7	0.0351	5 ± 2	14 ± 2	4 ± 2	0.1	0.93 ± 0.06
200	0.0804	10	0.0614	5 ± 2	16 ± 2	6 ± 3	0.2	0.95 ± 0.04

NaTDC

[BS] (mM)	Φ_{BS}	Charges (e)	$\Phi_{Software}$	R_{Pol} (Å)	R_{Eq} (Å)	$V_{Micelle\ core}$ (nm ³)	$x_{Water\ in\ the\ core}$	Eccentricity
10	0.0032	3	0.0027	5 ± 2	14 ± 2	4 ± 2	0.2	0.93 ± 0.06
25	0.0091	7	0.0076	6 ± 2	16 ± 2	6 ± 3	0.2	0.93 ± 0.05
30	0.0111	7	0.0093	7 ± 2	16 ± 2	7 ± 3	0.2	0.90 ± 0.07
50	0.0190	10	0.0154	7 ± 2	17 ± 2	8 ± 3	0.2	0.91 ± 0.06
100	0.0387	15	0.0310	8 ± 2	18 ± 2	11 ± 4	0.2	0.90 ± 0.06
200	0.0783	19	0.0626	8 ± 2	21 ± 2	14 ± 5	0.2	0.92 ± 0.04

With salt

NaTC

[BS] (mM)	Φ_{BS}	Charges (e)		$\Phi_{Software}$		R_{Pol} (Å)		R_{Eq} (Å)		$V_{Micelle\ core}$ (nm ³)	$V_{Micelle}$ (nm ³)	$x_{Water\ in\ the\ core}$	$x_{Water\ in\ micelles}$	Eccentricity		$\Phi_{Micelles}$	N_{agg}
		SANS	SAXS	SANS	SAXS	SANS	SAXS	SANS	SAXS	SANS	SAXS	SANS	SAXS	SANS	SAXS	SAXS	SAXS
4	0.0008		-		0.0005		4 ± 2		8 ± 2		1 ± 1		0.4		0.87 ± 0.16	0.0013	1 ± 1
7	0.0021		-		0.0007		3 ± 2		11 ± 2		1 ± 1		0.7		0.96 ± 0.05	0.0060	1 ± 1
10	0.0033	-	-	0.0031	0.0008	3 ± 2	4 ± 2	9 ± 2	14 ± 2	1 ± 1	3 ± 2	0.1	0.8	0.94 ± 0.08	0.96 ± 0.04	0.0135	1 ± 1
20	0.0074		-		0.0017		7 ± 2		16 ± 2		7 ± 3		0.8		0.90 ± 0.07	0.0321	2 ± 1
25	0.0094	-		0.0083		3 ± 2		13 ± 2		2 ± 2		0.1		0.97 ± 0.04			
50	0.0197	-	-	0.0146	0.0047	5 ± 2	11 ± 2	12 ± 2	15 ± 2	3 ± 2	10 ± 3	0.3	0.8	0.91 ± 0.08	0.68 ± 0.18	0.0826	4 ± 1

NaTDC

[BS] (mM)	Φ_{BS}	Charges (e)		$\Phi_{Software}$		R_{Pol} (Å)		R_{Eq} (Å)		$V_{Micelle\ core}$ (nm ³)	$V_{Micelle}$ (nm ³)	$x_{Water\ in\ the\ core}$	$x_{Water\ in\ micelles}$	Eccentricity		$\Phi_{Micelles}$	N_{agg}
		SANS	SAXS	SANS	SAXS	SANS	SAXS	SANS	SAXS	SANS	SAXS	SANS	SAXS	SANS	SAXS	SAXS	SAXS
2	0.0004		-		0.0001		6 ± 2		22 ± 2		13 ± 6		0.7		0.96 ± 0.03	0.0011	7 ± 3
5	0.0016		-		0.0004		11 ± 2		23 ± 2		24 ± 6		0.8		0.88 ± 0.05	0.0062	9 ± 2
10	0.0036	-	-	0.0028	0.0007	8 ± 2	14 ± 2	19 ± 2	23 ± 2	12 ± 4	30 ± 7	0.2	0.8	0.91 ± 0.05	0.79 ± 0.08	0.0181	9 ± 2
20	0.0075		-		0.0017		18 ± 2		21 ± 2		32 ± 7		0.8		0.52 ± 0.21	0.0332	11 ± 2
25	0.0095	-		0.0069		9 ± 2		18 ± 2		12 ± 4		0.3		0.87 ± 0.07			
30	0.0115	-		0.0082		9 ± 2		18 ± 2		13 ± 4		0.3		0.87 ± 0.07			
50	0.0194	-	-	0.0140	0.0045	11 ± 2	21 ± 2	17 ± 2	19 ± 2	13 ± 4	31 ± 6	0.3	0.8	0.76 ± 0.12	0.43 ± 0.27	0.0833	11 ± 2

Scattering data obtained for BS micelles at 37°C

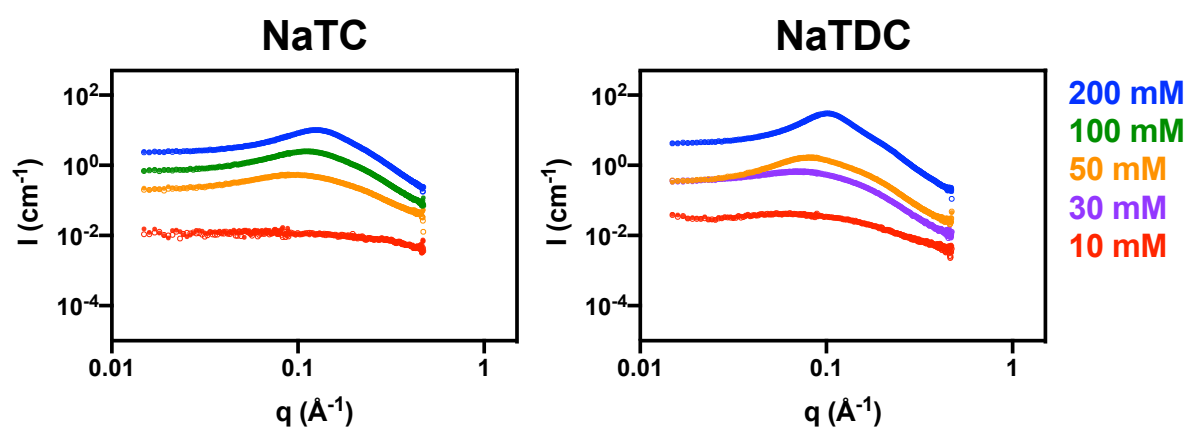


Figure S5: Scattered intensity (I) as a function of the scattering vector (q) for aqueous solutions of BS (NaTC, NaTDC), prepared at different concentrations (10, 30, 50, 100 and 200 mM) and measured at two different temperatures: (○) 25°C, (●) 37°C, without salt, with SANS. For readability purposes, curves are staggered vertically.

MD simulations data obtained for BS micelles

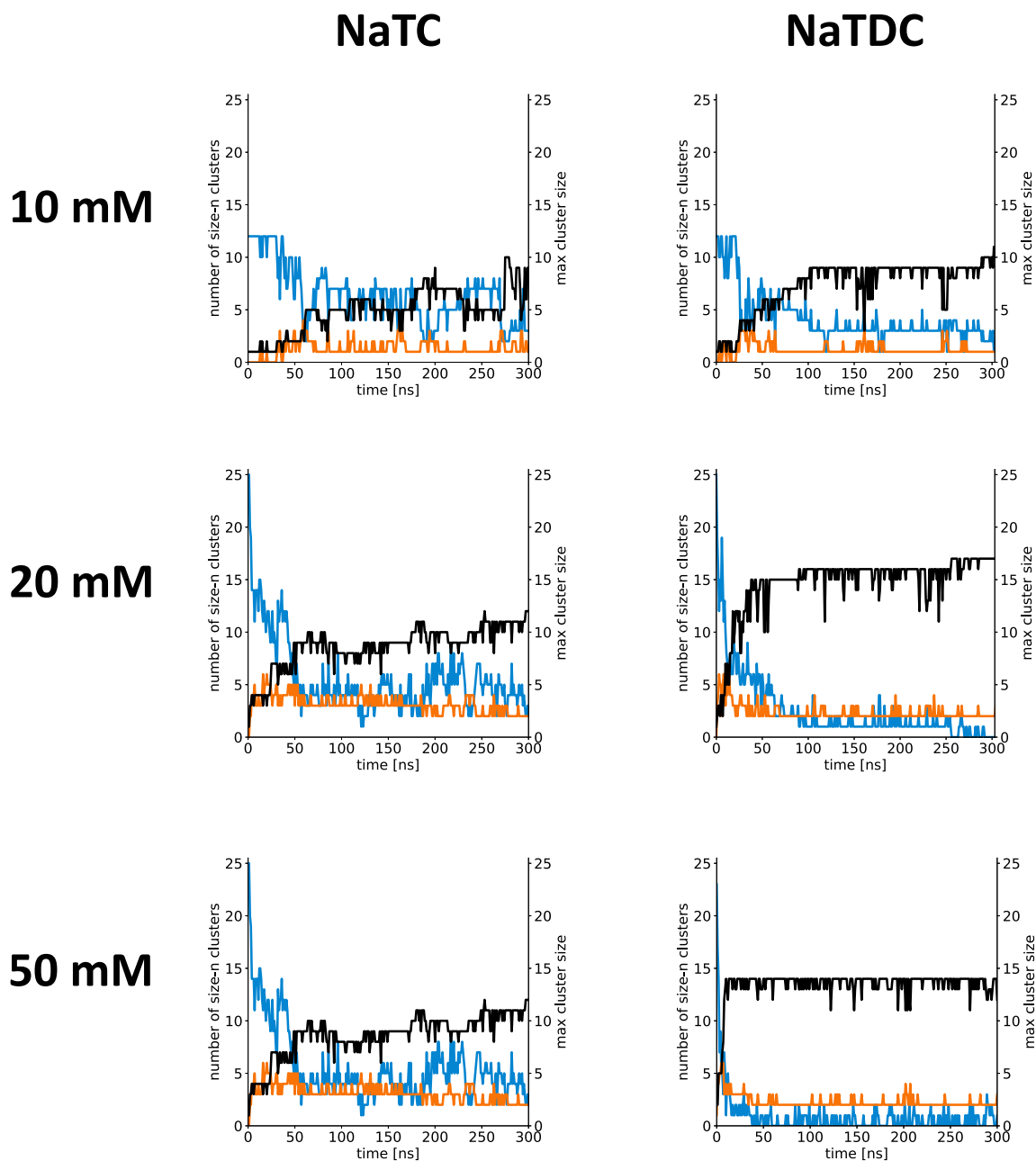


Figure S6: Number of BS clusters containing two or more BS molecules (—), number of free BS unimers in solution (—) and maximum number of BS molecules in one cluster (i.e., cluster size) (—) as a function of time, for the two BS (NaTC, NaTDC) at different concentrations (10, 20 and 50 mM), in the presence of 0.15 M NaCl.

Table S4: Average eccentricity (excluding and including unimers), radius of gyration (excluding and including unimers), number of isolated unimers, number of clusters (excluding unimers), average cluster size (excluding and including unimers) for aggregates containing more than one BS molecule (NaTC, NaTDC) in each of the simulated concentrations (10, 20 and 50 mM) of the BS in solution, in the presence of 0.15 M NaCl.

NaTC	10 mM	20 mM	50 mM
Eccentricity (excl. unimers)	0.30 ± 0.13	0.28 ± 0.12	0.34 ± 0.13
Eccentricity (incl. unimers)	0.68 ± 0.23	0.59 ± 0.27	0.55 ± 0.25
Radius of gyration (Å) (excl. unimers)	8.6 ± 1.2	9.6 ± 1.6	10.9 ± 2.2
Radius of gyration (Å) (incl. unimers)	6.4 ± 1.4	7.3 ± 2.1	8.4 ± 3.0
# isolated unimers	5.5 ± 1.7	4.3 ± 1.5	2.1 ± 1.3
# clusters (excl. unimers)	1.3 ± 0.6	3.0 ± 0.7	2.3 ± 0.6
Avg. cluster size (excl. unimers)	4.8 ± 2.1	7.0 ± 2.9	10.0 ± 4.5
Avg. cluster size (incl. unimers)	1.8 ± 1.8	3.4 ± 3.5	5.7 ± 5.5

NaTDC	10 mM	20 mM	50 mM
Eccentricity (excl. unimers)	0.22 ± 0.10	0.27 ± 0.09	0.25 ± 0.10
Eccentricity (incl. unimers)	0.48 ± 0.22	0.37 ± 0.18	0.32 ± 0.18
Radius of gyration (Å) (excl. unimers)	9.8 ± 1.1	10.7 ± 1.8	11.1 ± 1.0
Radius of gyration (Å) (incl. unimers)	6.6 ± 2.4	8.6 ± 3.2	9.9 ± 2.5
# isolated unimers	2.5 ± 1.1	1.3 ± 0.9	0.5 ± 0.7
# clusters (excl. unimers)	1.1 ± 0.4	2.2 ± 0.4	2.1 ± 0.4
Avg. cluster size (excl. unimers)	8.5 ± 2.4	10.9 ± 4.8	11.5 ± 2.7
Avg. cluster size (incl. unimers)	3.3 ± 3.7	7.3 ± 6.1	9.6 ± 4.8

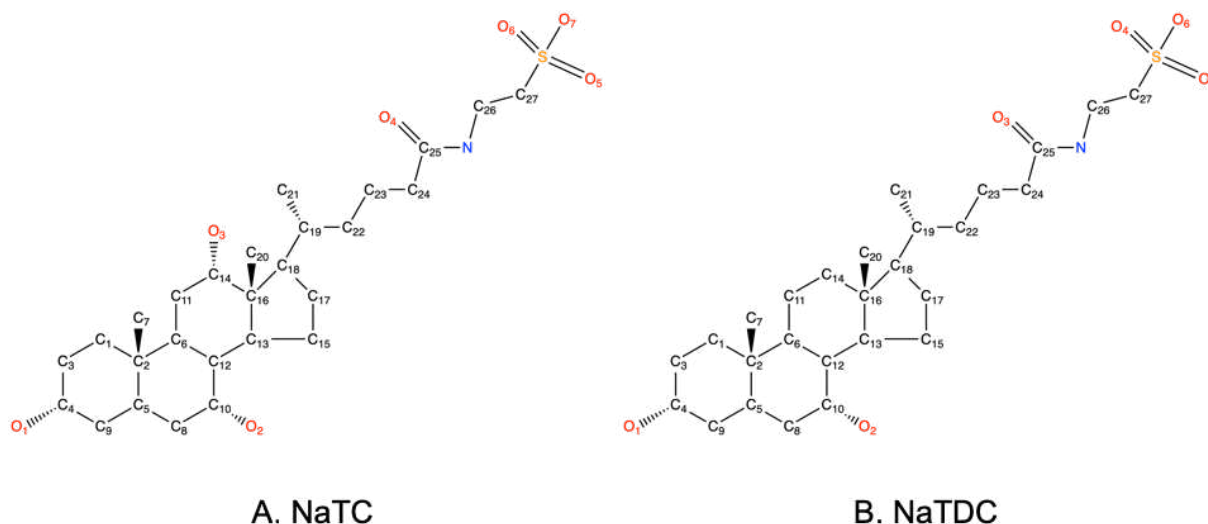


Figure S7: Definition of the atoms labels used in the interaction maps between molecules: A. NaTC, B. NaTDC.

In order to present the intermolecular interactions occurring between BS molecules in their micelles in a tractable manner, atom names were used in the manuscript for the heavy atoms in each BS. In Figure S7, we show the definition of these atom labels in terms of the chemical structure of each molecule.

Table S5: Radial distribution functions of water molecules around the various polar atoms in each BS molecule (NaTC, NaTDC). The first neighbour distance (r) and the coordination number of water molecules within the first hydration shell (n_c) are shown for each interaction at each of the three different concentrations (10, 20 and 50 mM), in the presence of 0.15 M NaCl. The atom labels used on the two axes are defined in Figure S7. O_w corresponds to the oxygen atom of the water molecule.

NaTC	10 mM		20 mM		50 mM	
	r (Å)	n_c	r (Å)	n_c	r (Å)	n_c
S - O_w	4.5	8.4	4.5	8.0	4.5	7.8
O_1 - O_w	3.6	3.8	3.6	3.5	3.6	3.4
O_2 - O_w	3.6	4.0	3.6	3.6	3.6	3.4
O_3 - O_w	3.6	4.4	3.6	4.0	3.6	3.9
O_4 - O_w	3.6	5.6	3.6	5.2	3.6	5.1

NaTDC	10 mM		20 mM		50 mM	
	r (Å)	n_c	r (Å)	n_c	r (Å)	n_c
S - O_w	4.5	8.0	4.5	8.1	4.5	8.1
O_1 - O_w	3.6	4.1	3.6	4.1	3.6	4.1
O_2 - O_w	3.6	4.4	3.6	4.4	3.6	4.5
O_3 - O_w	3.6	5.2	3.6	5.3	3.6	5.4

For both BS, the amide oxygen (O_4 for NaTC and O_3 for NaTDC) and sulfur (S) atoms of the ionic chain are the most hydrated polar atoms (more so than the oxygen atoms of the hydroxyl groups (Table S5)). Additionally, an increase in BS concentration results in a lower extent of

hydration around NaTC polar atoms, a 10% decrease being observed when comparing BS micelles formed at 10 and 50 mM; in contrast, the polar atoms of NaTDC remain equally hydrated at all concentrations. The dehydration phenomenon observed with NaTC is attributed to the increasing number of interactions occurring between BS molecules as they further assemble with each other; as all the polar atoms are dehydrated by the same amount, there does not seem to be any region of the NaTC molecule that is preferably shielded during the self-aggregation process. The lack of change in hydration content in NaTDC micelles suggests that the NaTDC polar oxygen atoms are not particularly involved in the interactions responsible for self-assembly; contrary to NaTC, there does not seem to be any competition for interaction with BS molecules between water and other BS molecules.

Scattering data obtained for BS mixed micelles (with FA or MAG)

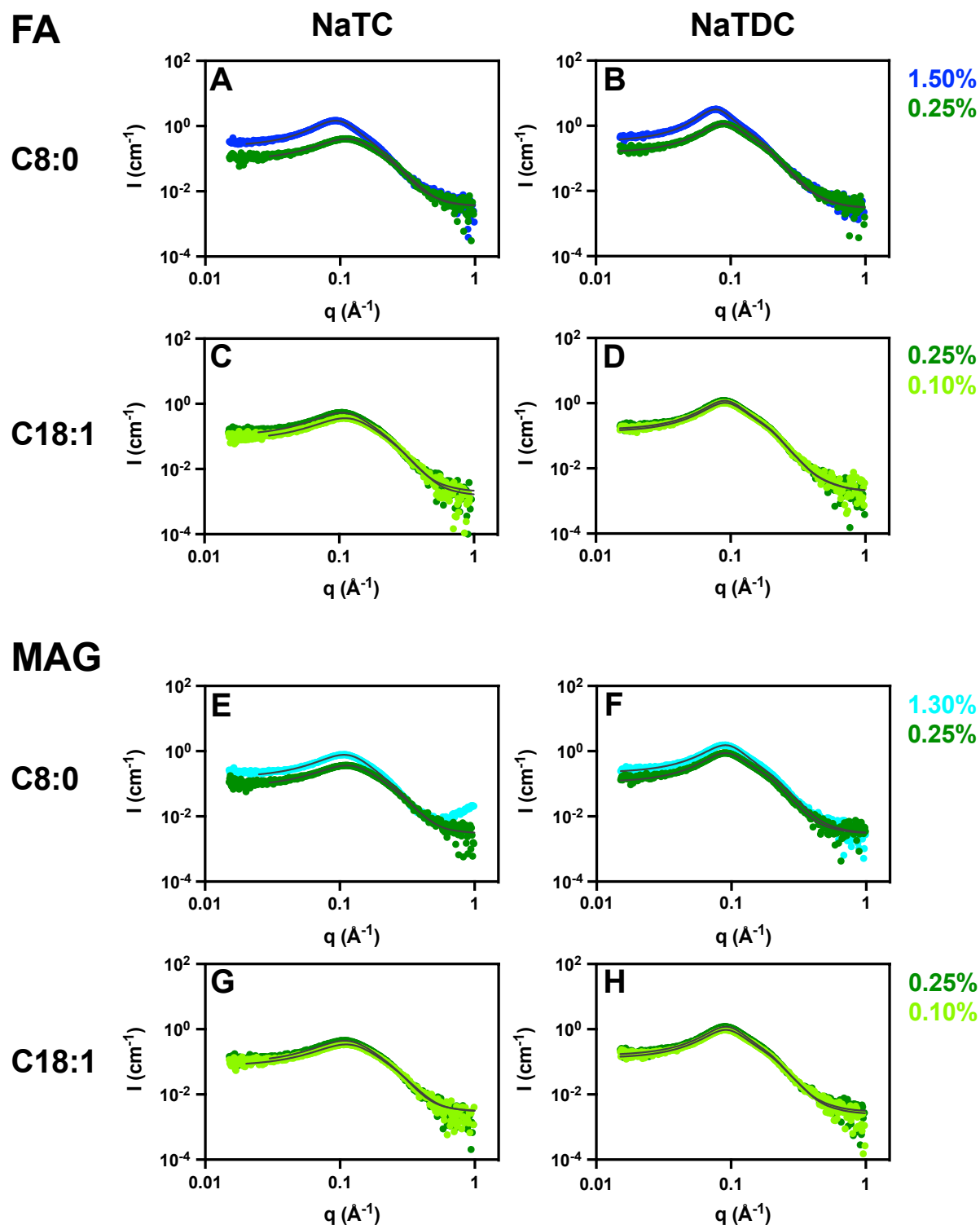


Figure S8: Scattered intensity (I) as a function of the scattering vector (q) for 100 mM BS aqueous solutions of either NaTC (A, C, E, G) or NaTDC (B, D, F, H), mixed with different amounts (from 0.10% to 1.50% w/w) of either FA (A, B, C, D) or MAG (E, F, G, H) and measured at 25°C, by SANS. Solutions were prepared without salt. Two types of FA: (A, B) C8:0, (C, D) C18:1, and MAG: (E, F) C8:0, (G, H) C18:1, were employed in this study. Solid lines correspond to fits to the data as described in the text (Equation (S3)).

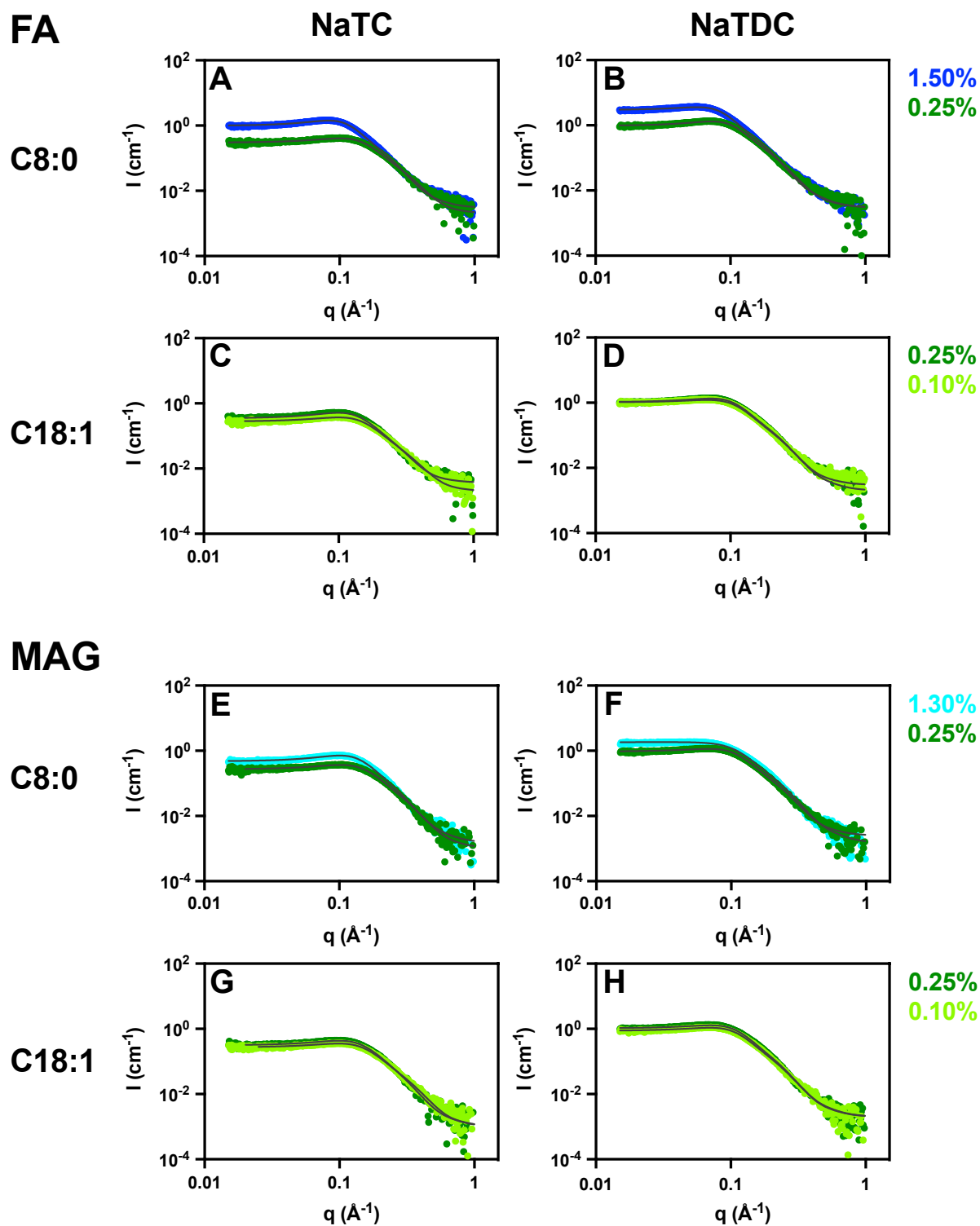


Figure S9: Scattered intensity (I) as a function of the scattering vector (q) for 100 mM BS aqueous solutions of either NaTC (A, C, E, G) or NaTDC (B, D, F, H), mixed with different amounts (from 0.10% to 1.50% w/w) of either FA (A, B, C, D) or MAG (E, F, G, H) and measured at 25°C, by SANS. Solutions were prepared with 0.15 M NaCl. Two types of FA: (A, B) C8:0, (C, D) C18:1, and MAG: (E, F) C8:0, (G, H) C18:1, were employed in this study. Solid lines correspond to fits to the data as described in the text (Equation (S3)).

Table S6: Concentration of FA (C8:0 or C18:1) or MAG (C8:0 or C18:1) in the sample ($[Additive]$), amount of charges in BS mixed micelle, volume fraction fitted by the software ($\Phi_{software}$), polar (R_{Pol}) and equatorial (R_{Eq}) radii values of the (oblate) ellipsoid BS mixed micelle, volume of the BS mixed micelle core ($V_{Mixed\ micelle\ core}$), for each BS studied: NaTC, NaTDC, with and without 0.15 M NaCl. These parameters were obtained from SANS2D data fitting.

NaTC		[Additive] (% w/w)	Charges (e)		$\Phi_{Software}$		R_{Pol} (Å)		R_{Eq} (Å)		$V_{Mixed\ micelle\ core}$ (nm ³)	
			No salt	Salt	No salt	Salt	No salt	Salt	No salt	Salt	No salt	Salt
No additive		0	7	-	0.0351	-	5 ± 2	-	14 ± 2	-	4 ± 2	-
FA	C8:0	0.25	8	12	0.0321	0.0347	6 ± 2	5 ± 2	15 ± 2	16 ± 2	5 ± 2	6 ± 3
		1.50	13	23	0.0456	0.0471	8 ± 2	10 ± 2	20 ± 2	31 ± 2	14 ± 5	41 ± 11
	C18:1	0.10	8	12	0.0290	0.0327	6 ± 2	5 ± 2	14 ± 2	16 ± 2	5 ± 2	6 ± 3
		0.25	9	16	0.0322	0.0332	7 ± 2	7 ± 2	15 ± 2	16 ± 2	7 ± 3	8 ± 3
MAG	C8:0	0.25	8	12	0.0309	0.0319	6 ± 2	6 ± 2	14 ± 2	15 ± 2	5 ± 2	6 ± 3
		1.30	9	15	0.0422	0.0418	7 ± 2	7 ± 2	16 ± 2	17 ± 2	8 ± 3	9 ± 4
	C18:1	0.10	8	12	0.0286	0.0314	6 ± 2	5 ± 2	14 ± 2	16 ± 2	5 ± 2	6 ± 3
		0.25	8	14	0.0305	0.0312	7 ± 2	7 ± 2	15 ± 2	16 ± 2	6 ± 3	7 ± 3

NaTDC		[Additive] (% w/w)	Charges (e)		$\Phi_{Software}$		R_{Pol} (Å)		R_{Eq} (Å)		$V_{Mixed\ micelle\ core}$ (nm ³)	
			No salt	Salt	No salt	Salt	No salt	Salt	No salt	Salt	No salt	Salt
No additive		0	15	-	0.0310	-	8 ± 2	-	18 ± 2	-	11 ± 4	-
FA	C8:0	0.25	17	30	0.0356	0.0359	8 ± 2	8 ± 2	20 ± 2	24 ± 2	13 ± 5	18 ± 6
		1.50	23	36	0.0473	0.0510	10 ± 2	10 ± 2	24 ± 2	31 ± 2	26 ± 7	41 ± 11
	C18:1	0.10	16	22	0.0331	0.0351	8 ± 2	8 ± 2	18 ± 2	23 ± 2	12 ± 4	18 ± 6
		0.25	17	26	0.0356	0.0377	9 ± 2	8 ± 2	19 ± 2	23 ± 2	13 ± 4	18 ± 6
MAG	C8:0	0.25	16	23	0.0294	0.0339	8 ± 2	8 ± 2	18 ± 2	23 ± 2	11 ± 4	17 ± 6
		1.30	15	13	0.0445	0.0435	8 ± 2	8 ± 2	21 ± 2	25 ± 2	15 ± 5	21 ± 7
	C18:1	0.10	16	24	0.0334	0.0327	8 ± 2	8 ± 2	19 ± 2	22 ± 2	11 ± 4	16 ± 5
		0.25	16	22	0.0370	0.0369	9 ± 2	8 ± 2	19 ± 2	23 ± 2	13 ± 4	18 ± 6

NR data obtained from TAG-incorporating liposomes bilayer

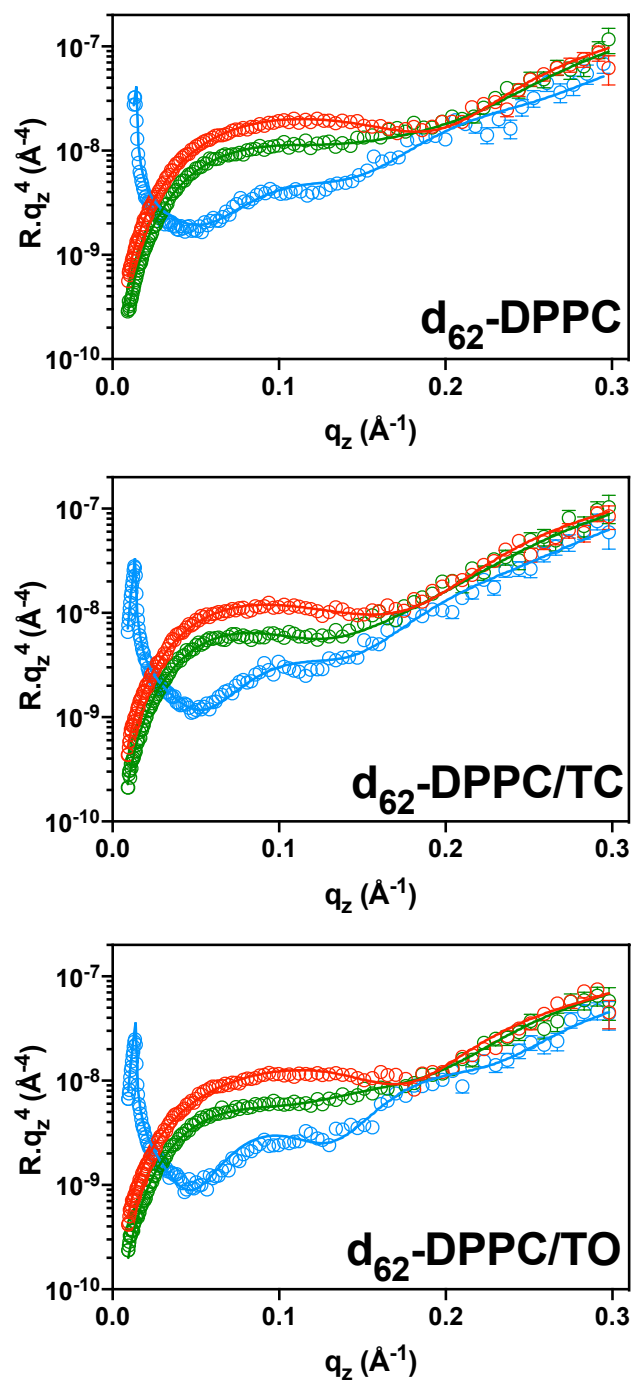


Figure S10: NR signal ($R \cdot q_z^4$ representation) of the TAG-incorporating SLB: d_{62} -DPPC, d_{62} -DPPC/TC, d_{62} -DPPC/TO, in different aqueous phases: (\circ) D_2O , (\circ) SiMW, (\circ) H_2O , as a function of the scattering vector (q_z).

		d ₆₂ -DPPC	d ₆₂ -DPPC/TC	d ₆₂ -DPPC/TO
SiO _x	σ (Å)	2.0	2.0	2.0
	t (Å)	8	8	8
	SLD ($\times 10^6$) (Å ⁻²)	3.41	3.41	3.41
	f_{water}	0	0	0
Water	σ (Å)	3.0	2.1	2.0
	t (Å)	4	5	4
	SLD ($\times 10^6$) (Å ⁻²)	0	0	0
	f_{water}	1	1	1
Head group	σ (Å)	2.5	4.4	3.8
	t (Å)	5	5	10
	SLD ($\times 10^6$) (Å ⁻²)	1.88	1.88	1.88
	f_{water}	0.06	0.06	0.4
Tails	σ (Å)	2.5	4.4	3.8
	t (Å)	15	15	16
	SLD ($\times 10^6$) (Å ⁻²)	6.71	6.41	5.77
	f_{water}	0.02	0	0.06
Additional TAG layer	σ (Å)	1.0	4.4	1.0
	t (Å)	-	2	-
	SLD ($\times 10^6$) (Å ⁻²)	-	-0.35	-
	f_{water}	-	0	-
Tails	σ (Å)	-	4.4	-
	t (Å)	15	15	16
	SLD ($\times 10^6$) (Å ⁻²)	6.71	6.41	5.77
	f_{water}	0.02	0	0.06
Head group	σ (Å)	2.5	4.4	3.8
	t (Å)	5	5	10
	SLD ($\times 10^6$) (Å ⁻²)	1.88	1.88	1.88
	f_{water}	0.06	0.06	0.4
	σ (Å)	2.5	4.4	3.8

Table S7: NR parameters of each upper and lower (tails and head group) layer of the lipid (d₆₂-DPPC, d₆₂-DPPC/TC, d₆₂-DPPC/TO) bilayer: σ , the roughness, t , the thickness, SLD , the scattering length density and f_{water} , the amount of water. The parameters of the silicon oxide (SiO_x) layer and water layer between the block and the upper head group region are also given. For d₆₂-DPPC/TC, an additional layer – corresponding to the incorporation of tricaprylin between d₆₂-DPPC tails – is present. For such a thin layer, the values of thickness (t) and roughness (σ) are strongly coupled and therefore, individual values are affected by a large error; however, the presence of this region in the midplane of the bilayer is unambiguous.

d₆₂-DPPC was found to form a symmetric SLB, with one homogeneous tails region and two hydrophilic head group layers. The latter were described by exactly the same structural parameters (t , SLD , f_{water}), while the interfacial roughness (σ) was allowed to be decoupled, because of differences likely to occur due to the different media faced by each hydrophilic layer (the solid silicon substrate for the upper layer, the aqueous phase for the lower one).

Several models were tested in order to reproduce the experimental reflectivity curves obtained for the d_{62} -DPPC/TC system: (i) the symmetric SLB model commonly used for pure lipids; (ii) a model in which tricaprylin would be partitioned between the hydrophobic and hydrophilic regions of the bilayer, and oriented parallel to the phospholipid acyl chains; and (iii) a model in which tricaprylin would exhibit a T shape and be localised at the centre of the bilayer, with two branches located between the two lipid tails regions (perpendicular to them) and one inserted among the tails (parallel to them). The model (iii) was the only one able to accurately fit the experimental data. It was possible to constrain the parameters of the head group layers to those of the pure d_{62} -DPPC SLB, while those of the tails regions and of the additional tricaprylin layer were allowed to vary during the fitting procedure. The incorporation of tricaprylin increased the interfacial roughness (σ) with respect to the one characterising the pristine d_{62} -DPPC SLB. The presence of the tricaprylin layer is particularly evident from the inspection of the *SLD* profiles reported in Figure 10A.

Considering the insertion of triolein into both lipid tails layers only (i.e., not into their head groups), data obtained for the d_{62} -DPPC/TO system were fitted with a traditional SLB model, with the parameters of the tails regions, as well as those of the head group layers, being let free to vary, and taking into account the presence of triolein molecules within the bilayer.

SANS data from TAG-incorporating liposomes

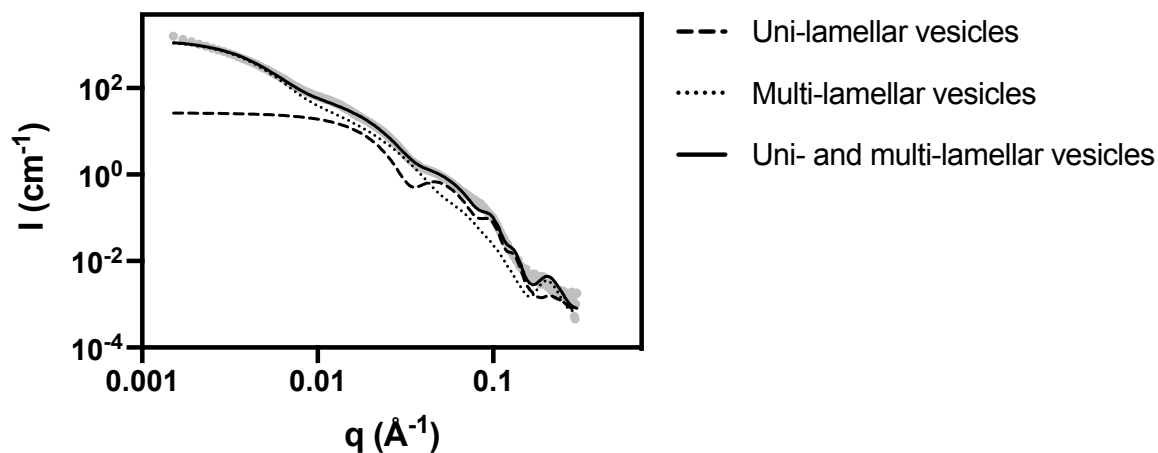


Figure S11: Scattered intensity (I) as a function of the scattering vector (q) for the pure DPPC vesicles (\bullet), measured at 25°C, by SANS. The connecting lines are the trend lines that best fit the data set using the vesicular model described in [18]; the contributions of both the uni- and multi-lamellar lipid vesicles are shown in this figure.

The structural organisation of DPPC liposomes was characterised using SANS (Figure S11). The change in slope observed at around 0.090 \AA^{-1} is characteristic of the presence of a bilayer, thereby indicating a core/shell (or vesicle) structure. The presence of two oscillations in the scattering intensity, at ca. 0.009 \AA^{-1} and 0.040 \AA^{-1} , could not be reproduced using either a uni- or multi-lamellar model alone. These features give an estimate of the size of the objects in solution (following this relation: $d \sim \frac{2\pi}{q}$): ca. 700 \AA and ca. 160 \AA , respectively. For this reason, we assumed two contributions: uni-lamellar vesicles (with a core radius of 6.70 nm (0.3 polydispersity) and an outer bilayer (or shell) thickness of 4.40 nm) and larger multi-lamellar liposomes (with an inner core radius of 17.5 nm (0.5 polydispersity) and 4 shells of 4.40 nm thickness each (0.7 polydispersity), separated by a 2.30 nm -thick gap of water).

Table S8: Amount of charges in BS mixed micelle, volume fraction fitted by the software ($\Phi_{software}$), polar (R_{Pol}) and equatorial (R_{Eq}) radii values of the (oblate) ellipsoid BS mixed micelle, volume of the BS mixed micelle core ($V_{Mixed\ micelle\ core}$), for the BS mixed micelles formed upon adding either 100 mM NaTC or 50 mM NaTDC, to the three different liposomes: DPPC, DPPC/TC, DPPC/TO. These parameters were obtained from the fits to D33 data obtained at 25°C.

Liposomes type	Charges (e)		$\Phi_{Software}$		R_{Pol} (Å)		R_{Eq} (Å)		$V_{Mixed\ micelle\ core}$ (nm ³)	
	NaTC	NaTDC	NaTC	NaTDC	NaTC	NaTDC	NaTC	NaTDC	NaTC	NaTDC
DPPC	8	13	0.0374	0.0241	8 ± 2	11 ± 2	17 ± 2	19 ± 2	9 ± 3	18 ± 3
DPPC/TC	8	13	0.0365	0.0245	7 ± 2	10 ± 2	17 ± 2	19 ± 2	9 ± 4	16 ± 4
DPPC/TO	8	11	0.0361	0.0239	8 ± 2	10 ± 2	16 ± 2	19 ± 2	9 ± 3	16 ± 3

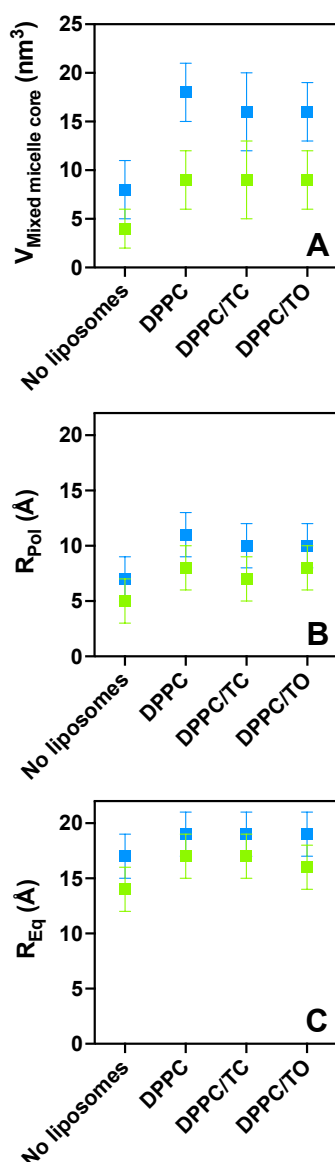


Figure S12: Evolution of (A) the volume of the BS mixed micelles obtained from SANS data ($V_{Mixed\ micelle\ core}$), (B) the polar radius of the BS mixed micelles (R_{Pol}) and (C) the equatorial radius of the BS mixed micelles (R_{Eq}), for various liposomes, with either (■) 100 mM NaTC or (■) 50 mM NaTDC. Results obtained with pristine BS micelles, in the absence of liposomes, are also indicated for comparison.

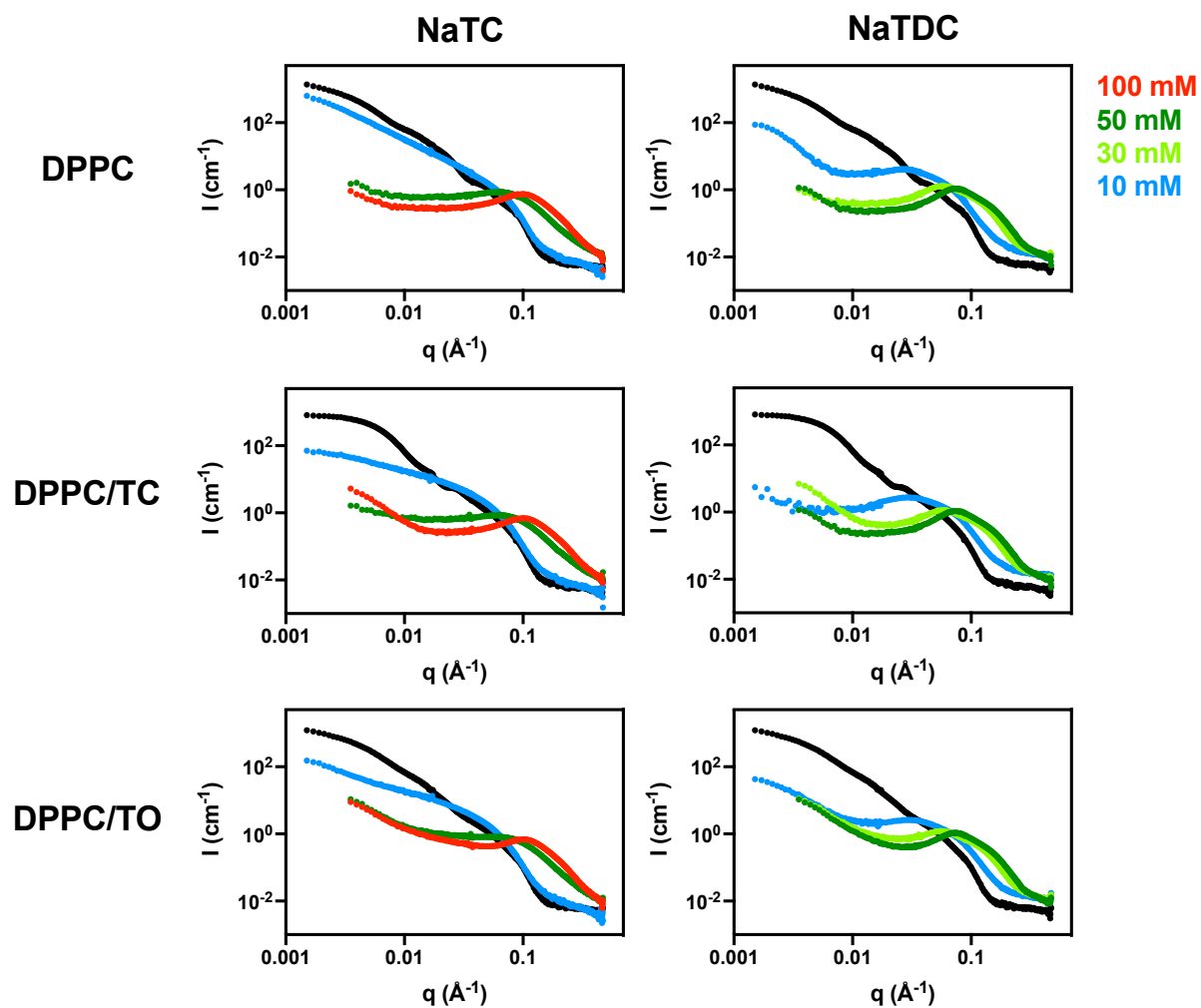


Figure S13: Scattered intensity (I) as a function of the scattering vector (q) for each TAG-incorporating lipid (DPPC, DPPC/TC, DPPC/TO) vesicle, mixed with different amounts (10, 30, 50 and 100 mM) of BS (NaTC, NaTDC), measured at 37°C, by SANS. The scattering curve of the pure liposomes (●) is also shown for comparison.

References

- [1] M.C. Dixon, Quartz crystal microbalance with dissipation monitoring: enabling real-time characterization of biological materials and their interactions., *J. Biomol. Tech.* 19 (2008) 151–158. <http://www.ncbi.nlm.nih.gov/pubmed/19137101>.
- [2] Y. Jing, H. Trefna, M. Persson, B. Kasemo, S. Svedhem, Formation of supported lipid bilayers on silica: relation to lipid phase transition temperature and liposome size, *Soft Matter*. 10 (2014) 187–195. doi:10.1039/C3SM50947H.
- [3] M. Rodahl, F. Höök, A. Krozer, P. Brzezinski, B. Kasemo, Quartz crystal microbalance setup for frequency and Q-factor measurements in gaseous and liquid environments, *Rev. Sci. Instrum.* 66 (1995) 3924–3930. doi:10.1063/1.1145396.
- [4] J. Webster, S. Holt, R. Dalgliesh, INTER the chemical interfaces reflectometer on target station 2 at ISIS, *Phys. B.* 385–386 (2006) 1164–1166. doi:10.1016/j.physb.2006.05.400.
- [5] O. Arnold, J.C. Bilheux, J.M. Borreguero, A. Buts, S.I. Campbell, L. Chapon, M. Doucet, N. Draper, R. Ferraz Leal, M.A. Gigg, V.E. Lynch, A. Markvardsen, D.J. Mikkelsen, R.L. Mikkelsen, R. Miller, K. Palmen, P. Parker, G. Passos, T.G. Perring, P.F. Peterson, S. Ren, M.A. Reuter, A.T. Savici, J.W. Taylor, R.J. Taylor, R. Tolchenov, W. Zhou, J. Zikovsky, Mantid - Data analysis and visualization package for neutron scattering and μ SR experiments, *Nucl. Instruments Methods Phys. Res. A.* 764 (2014) 156–166. doi:10.1016/j.nima.2014.07.029.
- [6] P. Van Vaerenbergh, J. Léonardon, M. Sztucki, P. Boesecke, J. Gorini, L. Claustre, F. Sever, J. Morse, T. Narayanan, An upgrade beamline for combined wide, small and ultra small-angle x-ray scattering at the ESRF, in: *AIP Conf. Proc.*, 2016: pp. 030034-1-030034–4. doi:10.1063/1.4952857.
- [7] R.K. Heenan, S.E. Rogers, D. Turner, A.E. Terry, J. Treadgold, S.M. King, Small angle neutron scattering using Sans2d, *Neutron News.* 22 (2011) 19–21. doi:10.1080/10448632.2011.569531.
- [8] D.F.R. Mildner, J.M. Carpenter, Optimization of the experimental resolution for small-

- angle scattering, *J. Appl. Crystallogr.* 17 (1984) 249–256. doi:10.1107/S0021889884011468.
- [9] C.D. Dewhurst, I. Grillo, D. Honecker, M. Bonnaud, M. Jacques, C. Amrouni, A. Perillo-Marcone, G. Manzin, R. Cubitt, The small-angle neutron scattering instrument D33 at the Institut Laue-Langevin, *J. Appl. Crystallogr.* 49 (2016) 1–14. doi:10.1107/S1600576715021792.
- [10] Institut Laue-Langevin, The LAMP software application available for the ILL spectrometers, (2018). <https://www.ill.eu/fr/users/support-labs-infrastructure/software-scientific-tools/lamp/> (accessed August 23, 2018).
- [11] L. Koester, H. Rauch, E. Seymann, Neutron scattering lengths: a survey of experimental data and methods, *At. Data Nucl. Data Tables.* 49 (1991) 65–120. doi:10.1016/0092-640X(91)90012-S.
- [12] V.F. Sears, Neutron scattering lengths and cross sections, *Neutron News.* 3 (1992) 26–37. doi:10.1080/10448639208218770.
- [13] Y. Gerelli, Aurore: new software for neutron reflectivity data analysis, *J. Appl. Crystallogr.* 49 (2016) 330–339. doi:10.1107/S1600576716000108.
- [14] Y. Gerelli, Phase transitions in a single supported phospholipid bilayer: real-time determination by neutron reflectometry, *Phys. Rev. Lett.* 122 (2019) 248101-1-248101–5. doi:10.1103/PhysRevLett.122.248101.
- [15] SasView for small angle scattering analysis, (2018). www.sasview.org (accessed August 22, 2018).
- [16] J.-P. Hansen, J.B. Hayter, A rescaled MSA structure factor for dilute charged colloidal dispersions, *Mol. Phys.* 46 (1982) 651–656. doi:10.1080/00268978200101471.
- [17] J.B. Hayter, J. Penfold, An analytic structure factor for macroion solutions, *Mol. Phys.* 42 (1981) 109–118. doi:10.1080/00268978100100091.
- [18] Y. Gerelli, M.T. Di Bari, A. Deriu, L. Cantù, P. Colombo, C. Como, S. Motta, F. Sonvico, R.

May, Structure and organization of phospholipid/polysaccharide nanoparticles, *J. Phys. Condens. Matter.* 20 (2008) 104211–104218. doi:10.1088/0953-8984/20/10/104211.

- [19] D. Madenci, Study of the aggregation behaviour of egg yolk lecithin/bile salt mixtures by increasing the ionic strength, The University of Edinburgh, 2009. <http://hdl.handle.net/1842/4918>.
- [20] H. Matsuoka, J.P. Kratochvil, N. Ise, Small-angle X-ray scattering from solutions of bile salts: sodium taurodeoxycholate in aqueous electrolyte solutions, *J. Colloid Interface Sci.* 118 (1987) 387–396. doi:10.1016/0021-9797(87)90474-7.